

The Dynamics of Bimodular Continuous Attractor Neural Networks with Static and Moving Stimuli

Min Yan^{1,*}, Wen-Hao Zhang², He Wang^{1,3}, and K. Y. Michael Wong¹,

¹*Department of Physics, Hong Kong University of Science and Technology, Hong Kong SAR, P. R. China*

²*Department of Mathematics, University of Pittsburgh, USA*

³*Hong Kong University of Science and Technology Shenzhen Research Institute, Shenzhen 518057, China*

(Dated: October 17, 2019)

The brain achieves multisensory integration by combining the information received from different sensory inputs to yield inferences with higher speed or more accuracy. We consider a bimodular neural network each processing a modality of sensory input and interacting with each other. The dynamics of excitatory and inhibitory couplings between the two modules are studied with static and moving stimuli. The modules exhibit non-trivial interactive behaviors depending on the input strengths, their disparity and speed (for moving inputs), and the inter-modular couplings. They give rise to a family of models applicable to causal inference problems in neuroscience. They also provide a model for the experiment of motion-bounce illusion, yielding consistent results and predicting their robustness.

I. INTRODUCTION

The human brain is sophisticated and advanced. It performs computations efficiently [1–3]. The brain receives inputs from surrounding environment all the time via different sensory modalities, e.g., visual, auditory, olfactory and vestibular, and so on. Experiments showed that different cortical regions in the brain are not completely isolated from each other, and there exist interactions between different sensory modalities. When the brain is processing information, it is able to combine cues coming from different sensory modalities, producing responses with higher accuracy or speed. In addition, this kind of multisensory integration can also give rise to some interesting behaviors, such as sensory illusion and response enhancement.

Various models have been built to elucidate the information processing mechanism of the brain [4–10]. In this paper, we study the dynamics of bimodular Continuous Attractor Neural Networks (CANNs) [11–17]. CANNs have gained widespread attention due to their property of translational invariance of neuronal interactions, which endows the networks with the ability to hold a continuous family of stationary states [10–13]. This feature enables the network to track a moving stimulus continuously, providing a convincing model of processing continuous information in the brain.

The single-module CANNs have been studied extensively [14–17]. Nevertheless, our brain receives signals from more than one channels, such as visual, auditory, vestibular, olfactory, and so on. Experiments have found that the brain is organized in different modules, each playing a certain role in processing the information the brain receives [18, 19]. However, different modules in the brain interact with each other, enabling it to integrate the information it collects to get a comprehensive picture of the surroundings [20, 21]. Multisensory information processing has been investigated extensively in areas such as visual-auditory [22], visual-vestibular [23] or other kinds of combinations [24]. In this paper, we generalize the single-module CANNs to bimodular structure,

to simulate and explore the interactions between different sensory modalities in the brain. Compared with the single-module CANNs, bimodular networks are able to process information coming from different sensory modalities separately or simultaneously. As shown in this paper, by applying distinct inputs, the bimodular CANNs respond diversely. Furthermore, the couplings between the two neural modules also play vital roles during the information processing, especially when tracking a moving stimulus in one modality and a static stimulus in the other [25–27].

We compared the theoretical predictions of the bimodular CANNs with the experiments in which different sensory modalities are involved during information processing, e.g., sensory illusions [28–30]. In this paper we study the Motion-Bounce Illusion experiment, which incorporates visual and auditory sensory modalities [22, 31, 32], and show that sensory inputs from one modality can affect the perception of stimuli in another modality, consistent with experimental results.

II. NETWORK ARCHITECTURE

A. Single Layer CANNs

We first describe single-module CANNs which process a one-dimensional stimulus. The stimulus can be regarded as the position or moving direction of an object, or head direction or other continuous variables. Each neuron in the network has its own preferred stimulus (direction), hence the whole network can encode all the stimuli information in the population of neurons. We use $U(x, t)$ to denote the synaptic input at time t to the neurons whose preferred stimulus is x , and $x \in [0, 2\pi)$. The dynamics of the $U(x, t)$ is [14–16]

$$\tau \frac{\partial U(x, t)}{\partial t} = -U(x, t) + \rho \int_{-\infty}^{\infty} J(x, x') r(x', t) dx' + I_{ext}(x, t), \quad (1)$$

where τ is a time constant, controlling the rate at which the synaptic input decays to the total input of the neuron, typically of the order of 1 ms. The function $I_{ext}(x, t)$ denotes the external input to the network at time t and position x , and ρ is the density of neurons. The couplings between the neurons located at positions x and x' are denoted as Gaussian functions $J(x, x')$:

$$J(x, x') = \frac{J_0}{\sqrt{2\pi}a} \exp\left[-\frac{(x-x')^2}{2a^2}\right], \quad (2)$$

where a defines the interaction range among the neurons. It can be seen from Eq.(2) that the coupling is translational invariant, so the coupling depends on the displacement $x - x'$ (modulo 2π for angular variables). This endows the network the ability to support a continuous family of attractors. The function $r(x, t)$ denotes the firing rate at time t and position x :

$$r(x, t) = \frac{[U(x, t)]_+^2}{1 + k\rho \int_{-\infty}^{\infty} [U(x', t)]_+^2 dx'}, \quad (3)$$

in which $[U]_+ \equiv \max(U, 0)$, and k is the global inhibition, which controls the extent to which the firing rate saturates [33].

Before applying external stimuli to the neural network, we first consider the intrinsic dynamics of the CANNs without external inputs ($I_{ext} = 0$). For $0 < k < k_c \equiv J_0^2 \rho / (8\sqrt{2\pi}a)$ and for $a \ll 2\pi$, the CANNs support a continuous family of stationary states (plotted in Fig. 1), denoted as:

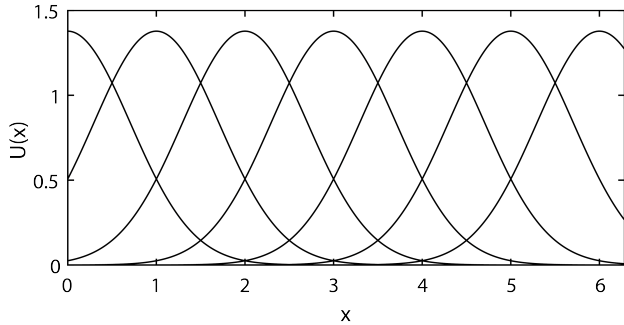


FIG. 1. The stationary states of the CANNs when there is no external input. They are also the solutions of Eq. (1) under $I_{ext}(x, t) = 0$.

$$\tilde{U}(x|z) = U_0 \exp\left[-\frac{(x-z)^2}{4a^2}\right], \quad (4)$$

$$\tilde{r}(x|z) = r_0 \exp\left[-\frac{(x-z)^2}{2a^2}\right], \quad (5)$$

where $U_0 = [1 + (1 - k/k_c)^{1/2}] J_0 / (4\sqrt{\pi}ak)$, $r_0 = [1 + (1 - k/k_c)^{1/2}] / (2\sqrt{2\pi}ak\rho)$, and z is a free parameter denoting the peak position of the Gaussian bump.

To simplify, we rescale the parameters: $\tilde{U} = \rho J_0 U$, $\tilde{I}_{ext} = \rho J_0 I_{ext}$, $\tilde{r} = (\rho J_0)^2 r$, $\tilde{k} = \frac{8\sqrt{2\pi}ak}{\rho J_0^2}$. Then Eq. (1) and Eq. (3) can be rewritten as:

$$\tau \frac{\partial \tilde{U}(x, t)}{\partial t} = -\tilde{U}(x, t) + \int_{-\infty}^{\infty} \frac{J(x, x')}{J_0} \tilde{r}(x', t) dx' + \tilde{I}_{ext}(x, t), \quad (6)$$

$$\tilde{r}(x, t) = \frac{[\tilde{U}(x, t)]_+^2}{1 + \frac{\tilde{k}}{8\sqrt{2\pi}a} \int_{-\infty}^{\infty} dx' [\tilde{U}(x', t)]_+^2}. \quad (7)$$

B. Bimodular CANNs

Now we generalize the single-module CANNs to a bimodular structure [34]. Since experiments have found that in the brain the different sensory modalities interact with each other during the information encoding process [35–39], we add couplings between the two modules in the bimodular CANNs. The network architecture is shown in Fig. 2. For simplification, consider the case that the neurons are evenly distributed in the two modules. Each neuron has its own preferred stimulus, indicated by the arrows in the neurons. Generalized from Eq.(6), the dynamical equations of the bimodular CANNs model are (for convenience, we use $U, r, k, I, J(x, x')$ to denote the rescaled variables $\tilde{U}, \tilde{r}, \tilde{k}, \tilde{I}, J(x, x')/J_0$ in the following of the paper):

$$\begin{aligned} \tau \frac{\partial U_1(x, t)}{\partial t} &= -U_1(x, t) + \omega_{11} \int_{-\infty}^{\infty} J_{11}(x, x') r_1(x', t) dx' \\ &\quad + \omega_{12} \int_{-\infty}^{\infty} J_{12}(x, x') r_2(x', t) dx' + I_{1ext}(x, t), \\ \tau \frac{\partial U_2(x, t)}{\partial t} &= -U_2(x, t) + \omega_{22} \int_{-\infty}^{\infty} J_{22}(x, x') r_2(x', t) dx' \\ &\quad + \omega_{21} \int_{-\infty}^{\infty} J_{21}(x, x') r_1(x', t) dx' + I_{2ext}(x, t). \end{aligned} \quad (8)$$

The recurrent coupling strength within module 1 (module 2) is denoted by ω_{11} (ω_{22}). The coupling from module 1 (module 2) to module 2 (module 1) is denoted by ω_{21} (ω_{12}). As for the coupling functions between two modules, we still adopt Gaussian functions similar to that in Eq. (2):

$$J_{ij}(x, x') = \frac{1}{\sqrt{2\pi}b} \exp\left[-\frac{(x-x')^2}{2b^2}\right], \quad i, j \in \{1, 2, i \neq j\}, \quad (9)$$

where b denotes the coupling width between two modules.

The firing rates (responses) in each module of bimod-

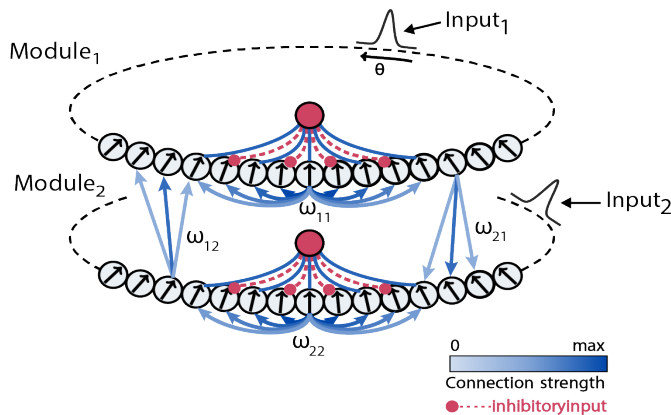


FIG. 2. The bimodular CANNs architecture.

ular CANNs are calculated

$$\begin{aligned} r_1(x, t) &= \frac{[U_1(x, t)]_+^2}{1 + \frac{k}{8\sqrt{2\pi}a} \int_{-\infty}^{\infty} dx' [U_1(x', t)]_+^2}, \\ r_2(x, t) &= \frac{[U_2(x, t)]_+^2}{1 + \frac{k}{8\sqrt{2\pi}a} \int_{-\infty}^{\infty} dx' [U_2(x', t)]_+^2}. \end{aligned} \quad (10)$$

There are also two external inputs I_{1ext} and I_{2ext} to the two modules respectively, which are set to be independent of each other. In this paper, both of the external stimuli are in Gaussian forms:

$$\begin{aligned} I_{1ext} &= I_{01} \exp \left[-\frac{(x - z_1)^2}{4a^2} \right], \\ I_{2ext} &= I_{02} \exp \left[-\frac{(x - z_2)^2}{4a^2} \right]. \end{aligned} \quad (11)$$

I_{01} and I_{02} denote the magnitudes of external inputs respectively, and x denote the positions of neurons. The central positions of inputs are denoted by z_1 and z_2 , which can be constants, and can also be variables depending on moving velocities, e.g., $z = vt$.

III. STATIC INPUTS

A. Dependence on Inter-Modular Couplings

Different inter-modular couplings can give rise to various dynamics of the neural network [26, 34]. We present the firing rates (responses) of the network as one example in Fig. 3 when there are only unidirectional couplings from module 1 to 2. The profile of the firing rate at an instant has a bump shape. External input I_{1ext} is a moving stimulus, and I_{2ext} is static. As shown in Fig. 3(b), after the response has been established at around position π , corresponding to its own input, it is dragged by the external input I_{1ext} soon after due to the excitatory coupling ω_{21} .

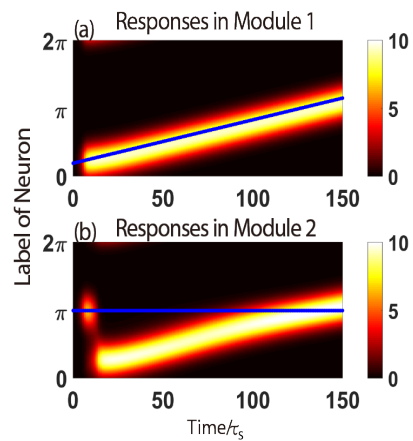


FIG. 3. The firing rates (responses) of bimodular CANNs when only unidirectional couplings from module 1 to 2. $\omega_{21} = 0.3$, $\omega_{12} = 0$. External inputs $I_{01} = I_{02} = 0.7$. I_{1ext} is moving at velocities of 0.02 rad/ms, and I_{2ext} is fixed at position of π . Blue dotted lines indicate trajectories of the central positions of inputs.

In general, bumps in the modules receiving excitatory inter-modular couplings are attracted, whereas those receiving inhibitory couplings are repelled. This gives rise to the various behaviors illustrated in Fig. 4. In Fig. 4(a), the bump in module 2 is attracted by module 1 to around position of external input 1, which results from the stronger inter-modular couplings ω_{21} .

In Fig. 4(b), the repulsive and inhibitory effects from module 2 to module 1 are evident in the responses of module 1, whose responses are pushed away from its input position. In the beginning the bump in module 2 is attracted by those in module 1 and deviate from position of I_{2ext} . Nevertheless, soon after the bump in module 1 is suppressed by module 2, the attraction effect disappears, and the bump in module 2 returns to follow its own input. In addition, the whole network spends longer time to reach steady state compared with that in Fig. 4(a).

Figure 4(c) presents the case when both inter-modular couplings are strongest, but ω_{21} is excitatory, and ω_{12} is inhibitory. In module 1, the responses are inhibited severely from the beginning, which also indirectly weakens the attractive effect from module 1 to module 2. After a short period, the responses in module 1 are completely inhibited, while the responses in module 2 are quickly established stably and strongly, almost not affected by module 1, due to the responses in module 1 being inhibited too quickly. Figure 4(d) chooses both inter-modular couplings to be inhibitory. The responses in both modules are comparable in magnitude, but are crippled by the prohibitive effects. Besides, both bumps deviate a little bit from its own input positions, resulting from the push effect, brought by the inhibitory inter-modular couplings. Figure 4(e) illustrates the situation when both inter-modular couplings are weak. The bump in module 1 is attracted towards to input 2 due to the excitatory ω_{12} . Likewise, the bump in module 2 is pushed away from its own input, given the inhibitory ω_{21} . How-

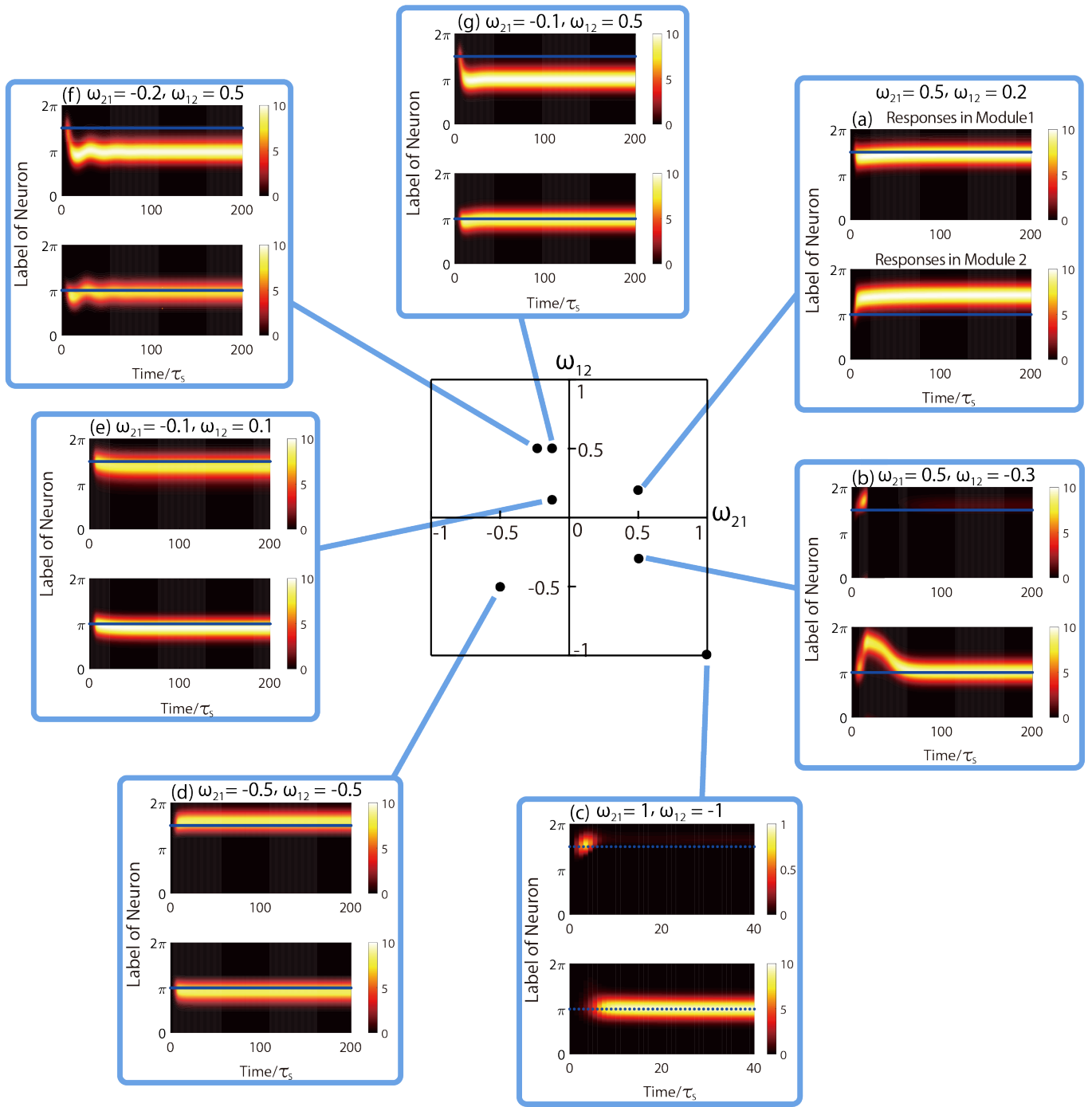


FIG. 4. The firing rates (responses) of bimodal CANNs when various inter-modular couplings are imposed. External inputs $I_{01} = I_{02} = 0.7$. I_{1ext} is fixed at position $3\pi/2$, and I_{2ext} is fixed at position π . Blue dotted lines indicate trajectories of inputs.

ever, the strengths of the responses are strange. Module 1 receives excitatory couplings from module 2, whereas its responses are weaker than those of module 2, which receives inhibitory couplings from module 1. Since the dynamics of the bimodal CANNs under weak inter-modular couplings behave differently from our forecast, we will study deeper in Fig. 6. Figures 4(f) and 4(g) share the same excitatory inter-modular coupling ω_{12} . Comparing the responses in both figures, it can be con-

cluded that the network applied with stronger inhibitory inter-modular coupling ω_{21} spends longer time reaching stable status. Besides, since the excitatory coupling ω_{12} is relatively much stronger than the inhibitory coupling ω_{21} , the responses in module 1 in both figures are all attracted approximately to input 2, and the strength of the responses are also enhanced by the excitatory inter-modular coupling. The bump in module 2 almost follows the input 2 in both cases, and the inhibitory effect from

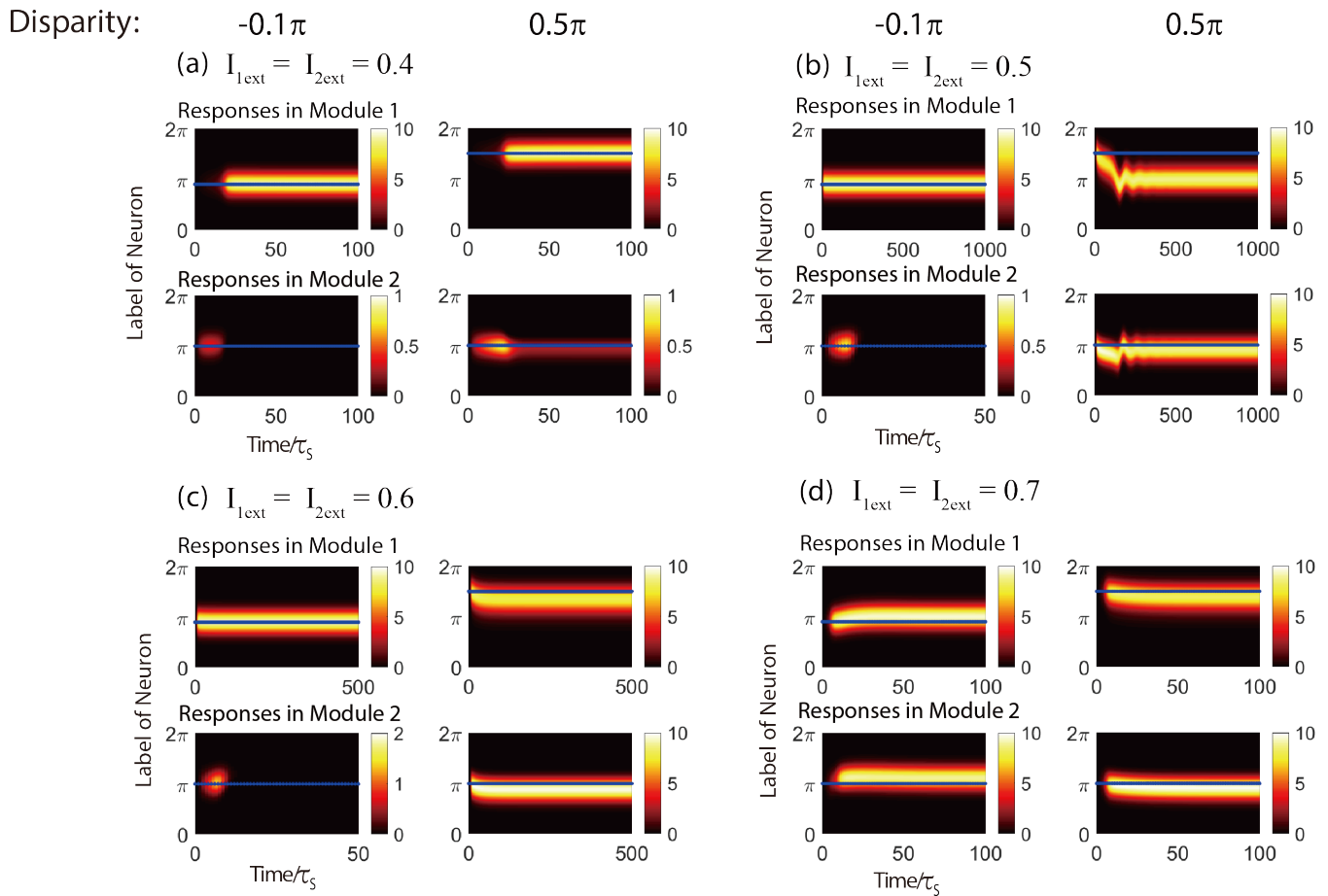


FIG. 5. Network behavior showing inhibitory effects at low disparity and bias effects at high disparity. The firing rates (responses) of the bimodular CANNs with $\omega_{21} = -0.1$ and $\omega_{12} = 0.1$ when the external input I_{1ext} locates at $[0.9\pi, 1.5\pi]$. I_{2ext} is fixed at position π . Blue dotted lines indicate trajectories of external inputs. The disparities between two external inputs ($L_1 - L_2$) are respectively in each column (listed at top line): -0.1π , 0.5π . (a) External inputs $I_{01} = I_{02} = 0.4$. (b) External inputs $I_{01} = I_{02} = 0.5$. (c) External inputs $I_{01} = I_{02} = 0.6$. (d) External inputs $I_{01} = I_{02} = 0.7$.

module 1 mainly reflects on the bump height which is obviously smaller than that of module 1.

B. Bias Effects

As shown in Fig. 4(e), when the inter-modular couplings ω_{21} and ω_{12} are both weak, especially when one of the couplings is inhibitory, and the other excitatory, the network behavior may appear anomalous. Figure 4(e) shows that module 1 receiving excitatory inter-modular coupling has weaker responses, compared with those in module 2 receiving inhibitory inter-modular coupling. In Fig. 5, we study further the network behavior with the same couplings as those in Fig. 4(e) ($\omega_{12} = 0.1, \omega_{21} = -0.1$), and with I_{1ext} located at $[0.9\pi, 1.5\pi]$ and I_{2ext} fixed at π .

A careful inspection of Fig. 5 for different disparities at different input strengths reveals that the network behavior is determined by the interplay of two effects. The first one is the inhibitory effect mainly effective at low disparity, as shown in Figs. 5(a) - 5(d). Under this condi-

tion the inhibitory inter-modular couplings suppress the responses in module 2, to the extent that they are totally suppressed after a short time for the weaker input strengths in Figs. 5(a) - 5(c). Even for the stronger input strengths in Fig. 5(d) when module 2 manages to sustain a stable response, its amplitude is still weaker than that in Fig. 5(d).

The second effect is the bias effect mainly operative at higher disparity, which explains the anomalous behavior in Fig. 4(e). Due to the inter-modular couplings, the peak positions of the bumps in both modules are either attracted or repelled from the respective stimulus positions. When the disparity is within the range of the inter-modular couplings, the tendency to displace the bumps increases with the disparity [15]. This displacement weakens the efficacy of the input stimuli and results in a reduction of the amplitude. Interestingly, due to the nonlinear dependence of the firing rate on the synaptic input, the bias due to an excitatory interaction is stronger than that of an inhibitory one. Thus the responses in module 1 (receiving excitatory interactions from module 2) have a stronger bias and a weaker amplitude.

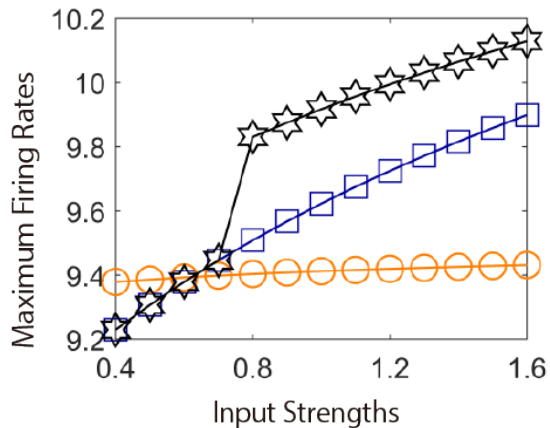


FIG. 6. The ‘inverse effectiveness’ in the bimodular CANNs. Y-axis denotes the maximum of the firing rates (r_1) of steady states of module 1. $\omega_{12} = 0.1, \omega_{21} = -0.1$. Square-lines stand for maximum firing rates in module 1 when it only receives external input I_{1ext} and no inputs from the other module. Circle-lines denote the maximum firing rates in module 1 only receiving inputs from module 2 via couplings, and $I_{1ext} = 0$. Star-lines record the maximum firing rates of steady states in module 1 when it receives both I_{1ext} and the inputs from module 2 via couplings. Disparity = 0.

Another observation about the network behavior is the principle of inverse effectiveness [40]. It states that the network response due to the combination of two inputs is weaker than the sum of the responses to the individual inputs, that is, network responses are sub-additive. This has been considered as an evidence of the divisive normalization of network responses, and was illustrated in bimodular networks with excitatory couplings [23]. As illustrated in Fig. 6, this principle is also valid for bimodular networks with excitatory and inhibitory couplings in respective directions.

C. Center of Mass Positions

In the convention of population coding, the brain infers the input positions through computing the center of mass of the firing rates of the neurons [41, 42]. Hence, it is convenient to illustrate the attraction and repulsion effects due to inter-modular couplings by tracing the center of mass positions of the bump. Its dependence on the disparity is plotted in Fig. 7, showing that the attraction and repulsion effects are strongest at low disparity, but the bumps become effectively independent at high disparity. In Fig. 7, we consider the case that the position of I_{2ext} is fixed, and its amplitude is fixed to be sufficiently strong for the network to reach steady state in a short time, but also sufficiently moderate for the network to exhibit competition effects.

In Fig. 7(a), both of the inter-modular couplings are weak excitatory, namely, the two modules attract and excite each other. Therefore the output positions of module 1 are much closer to I_{2ext} (position π) when I_{1ext} is

weaker than I_{2ext} . When I_{1ext} increases to 0.6, the output position begins to approximate to its own input, and the output dotted curves approaches the diagonal dashed line, which indicates that the output position of module 1 is approaching its own input. However, attracted by the module 2, the output position of module 1 cannot fully overlap with its stimulus.

Figure 7(b) shows the situation when the coupling from module 1 to module 2 is excitatory while the coupling in the reverse direction is inhibitory. When the external input I_{1ext} is weaker than the I_{2ext} , the repulsion effect arising from inhibitory couplings dominates the behaviors, so that the output positions of module 1 are pushed away from its corresponding input positions. This effect becomes gradually prominent when the I_{1ext} position approaches position π , and reaches maximum when the I_{1ext} is applied at π . As the external input I_{1ext} increases to 0.7, equivalent to I_{2ext} strength, the input 1 is strong enough to move against the repulsion from module 2, pulling the output positions of module 1 towards its own input positions.

In Fig. 7(c), the roles of the couplings in Fig. 7(b) are exchanged. Now module 1 inhibits module 2, and module 2 attracts module 1. Similarly, when input 1 is weaker than input 2, the inhibition acting on module 2 is also weak. Then input 2 is able to exert its attraction on module 1, resulting in output positions of module 1 staying close to input 2 position π . For clarity and accuracy, Fig. 7(d) amplifies the dotted curves in Fig. 7(c) for the amplitude of I_{1ext} in the range 0.1 to 0.4. When the amplitude I_{01} of I_{1ext} increases to 0.5 and 0.6, the output position in module 1 remains affected by input 2 at low disparity, but eventually jumps discontinuously to track input 1 at high disparity. For I_{01} lying between 0.6 and 0.7, we can find a continuous variation of the output position when the disparity changes. When I_{01} becomes 0.7 or above, it has sufficient strength to suppress responses in module 2 at low disparity, but responses appear in module 2 at high disparity, resulting in a jump from fully tracking input 1 to output positions between inputs 1 and 2.

D. Relevance to Causal Inference

The behaviors of the proposed bimodular networks are relevant to models of causal inference in the brain [43]. Causal inference refers to the process of inferring whether or not an event A is caused by another event B. In normative models of causal inference for two channels using a model averaging strategy, cues from these channels are integrated at low disparity, resulting in an averaged prediction. However, when the disparity is too high, the stimuli of the individual channels are inferred to be independent. This picture is valid for a wide range of prior distributions, and the resultant inference resembles the output position in Fig. 7(a) for bimodular networks connected by excitatory couplings.

Bimodular networks with a pair of excitatory and in-

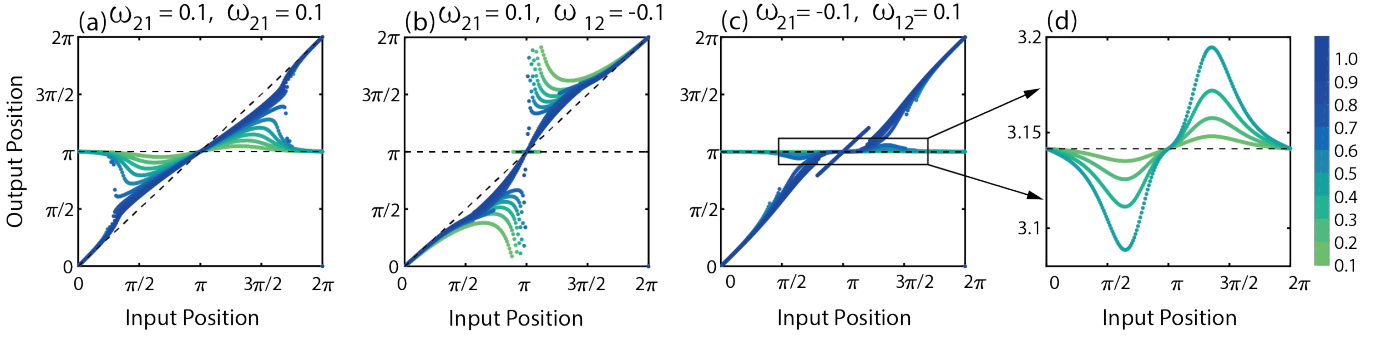


FIG. 7. The center of mass of responses in module 1 (denoted as output position) versus the input position of module 1 under different weak inter-modular couplings. External input I_{2ext} is fixed at position π and amplitude of 0.7. I_{01} strengthens from 0.1 to 1.0, indicated by colorbar. (a) Inter-modular couplings $\omega_{21} = \omega_{12} = 0.1$. (b) Inter-modular couplings $\omega_{21} = 0.1, \omega_{12} = -0.1$. (c) Inter-modular couplings $\omega_{21} = -0.1, \omega_{12} = 0.1$. (d) Amplifying the parts of I_{1ext} amplitude ranging among $[0.1, 0.4]$.

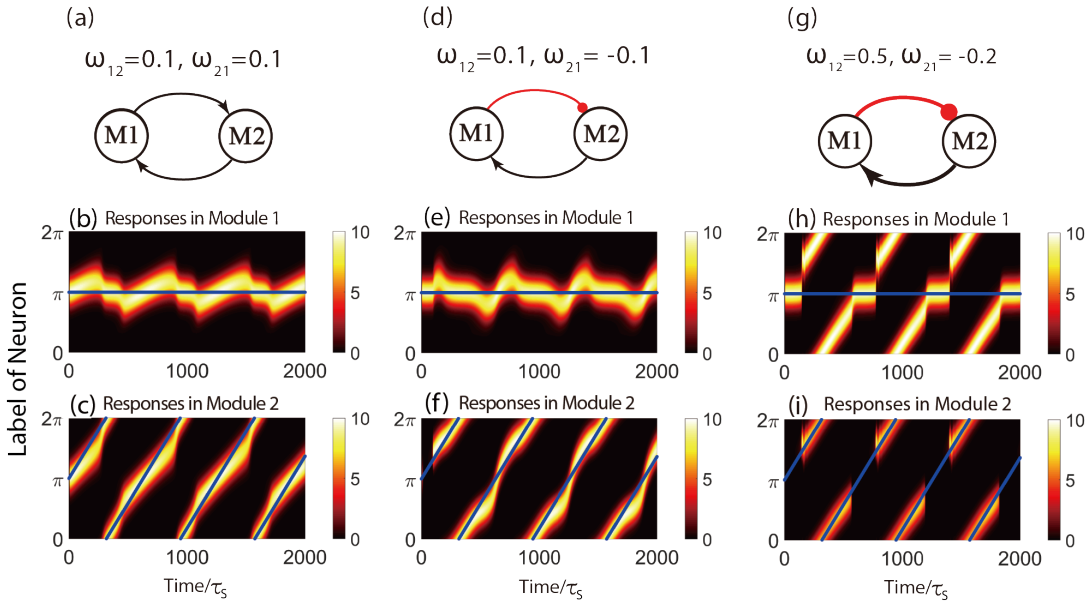


FIG. 8. The firing rates (responses) of bimodular CANNs under different weak inter-modular couplings and stimuli, one static and one moving. I_{1ext} is static and located at position π . I_{2ext} is a moving stimulus, moving velocity $v_2 = 0.01$ rad/ms. Blue dotted lines indicate the inputs trajectories. $k = 0.7$ and $I_{01} = I_{02} = 0.7$ except $I_{02} = 1.4$ in (g), (h) and (i). (a), (d), and (g) The sketches of the network structure. M_1 denotes module 1, and M_2 denotes module 2. (b), (e) and (h) The firing rates (responses) of module 1 under different inter-modular couplings. (c), (f), and (i) The firing rates (responses) of module 2 under different inter-modular couplings.

hibitory inter-modular couplings also belong to the same class of causal inference models. These models use a Bayesian framework which consists of the prior distribution of the bimodular stimuli and the likelihood distribution of the cues generated from the stimuli. There are cases that the input from one channel is subordinate to the other. For example, the likelihood distribution of the subordinate channel may be correlated with that of the other channel and has a higher uncertainty. As shown in Appendix, the optimal network structure in this case consists of a pair of excitatory and inhibitory couplings, and the module with the subordinate input is similar to module 1 in Fig. 7(c), yielding the same output as module 2 at low disparity.

IV. MOVING INPUTS

A. Dynamical Behaviors

In practice, the information input to the brain is typically dynamical. In unimodular networks, a rich spectrum of behaviors is already observed [4]. Therefore it is instructive to study the processing of moving stimuli in bimodular CANNs. Following the previous section, we consider external inputs of moderate strengths.

In Fig. 8, the external inputs I_{1ext} and I_{2ext} are applied from time $t \geq 0$, indicated by blue dotted lines. Input 1 remains static while input 2 begins to move thereafter. Figures 8(b) and 8(c) (8(e) and 8(f)) correspond

to the inter-modular couplings in Fig. 8(a)(8(d)). As Figs. 8(a) and 8(d) show, module 1 is heavily influenced by the module 2, owing to the excitatory inter-modular couplings ω_{12} . Under the excitatory ω_{12} , the responses in module 1 in Fig. 8(b) and 8(e) are oscillating around the input 1 position. There are some differences in the beginning stage of the dynamics of Figs. 8(b) and 8(e). In Fig. 8(b), since ω_{12} and ω_{21} are both excitatory, the responses in module 1 at beginning are attracted by input 2. After input 2 moves away, its attractive effect on module 1 is reduced, and the bump in module 1 moves back to position π , completing a cycle of oscillation. On the other hand, in Fig. 8(e), ω_{21} is inhibitory. Hence, the bump in module 2 is inhibited at the beginning, which also gives module 1 chances to follow input 1 tightly and free from the attractive effect. Once the responses in module 2 are established, the bump in module 1 is immediately repelled from its own input, and when input 2 moves too far away to exert its influence, the bump in module 1 again returns to position π . In Figs. 8(c) and 8(f), the couplings from module 1 to module 2 (ω_{21}) are different, while the influenced sites are the same (around π), where the external input 1 locates. Therefore in Fig. 8(c), the responses of module 2 at position around π are enhanced, resulting from the positive couplings ω_{21} . In Fig. 8(f), the ω_{21} is inhibitory, thus the responses of module 2 are inhibited around the position π .

Figures 8(a)-8(f) show that the static and moving stimuli can interact with each other via the couplings between two modules. In addition, the competition between the external inputs is apparent in module 1, while input 1 is direct and input 2 works via inter-modular couplings. In Figs. 8(b) and 8(e), the bump in module 1 follows the moving input 2 at regular intervals, giving rise to the oscillation patterns. In order to illustrate the competition, we present a relatively extreme situation, shown in Figs. 8(g)-8(i).

Figures 8(g)-8(i) show the dynamics of the bimodular CANNs under a stronger excitatory inter-modular coupling (ω_{12}) accompanied by a weaker inhibitory coupling (ω_{21}), as shown in Fig. 8(g). The input amplitude of the static input is much stronger than that of the moving input. Now the dynamics of the network are totally different from that in Figs. 8(d) - 8(f). In Fig. 8(i), on account of the strong inhibitory couplings from module 1, the responses in module 2 around the position π are almost fully suppressed. Only after input 2 has moved away or before it arrives at the position π can stable and strong responses be built in module 2. However, influenced by the strong attraction from module 2, the responses in module 1 can only sustain its static state when the responses in module 2 are inhibited. When the responses in module 2 are rebuilt, they again attract the responses in module 1, inducing the module 1 to track the moving I_{2ext} instead of its own static input I_{1ext} .

B. Phase Diagrams

The different cases in Fig. 8 illustrate the effects of the competition between two external inputs and the effects of inter-modular couplings on the dynamical behaviors. To obtain a more comprehensive picture, we introduce the tracking mean square deviations with respect to the static and moving inputs as references. A comparison of their magnitudes reveals whether the responses are tracking the static or moving inputs. Below, we denote the modules receiving static and moving inputs as modules s and m respectively. Since module m receives a moving stimulus, we particularly focus on the mean square deviations in module m ,

$$\begin{aligned}\sigma_s^2 &= \langle (x_m(t) - v_s t)^2 \rangle_t - \langle x_m(t) - v_s t \rangle_t^2, \\ \sigma_m^2 &= \langle (x_m(t) - v_m t)^2 \rangle_t - \langle x_m(t) - v_m t \rangle_t^2,\end{aligned}\quad (12)$$

where $x_m(t)$ denotes the center of mass of the responses in module m , $v_m(v_s)$ indicates the moving velocities of two external inputs, and $v_s = 0$. $\langle \dots \rangle_t$ represents average over time. σ_m^2 and σ_s^2 denote the mean square deviations of the responses in module m with respect to two external input positions to the network. When σ_s^2 is less than σ_m^2 , it means the module m is tracking the static input more than its own moving input. Otherwise, it tracks the moving input more.

Figure 9 shows the phase diagrams of tracking behaviors. Three kinds of couplings are listed at upper left corner, respectively. Excitatory inter-modular couplings are denoted by arrows, and inhibitory couplings are denoted by red circles. We also pick some points with the same moving velocities, but various moving input strengths as examples of the responses in module m shown in Fig. 9. The bump in module s is effectively pinned to the static input in this parameter range and will not be shown. The corresponding data points are marked in Figs. 9(a), 9(d) and 9(j) respectively by black stars.

In three groups of couplings, the module m cannot track its own moving stimulus when the stimulus is relatively weak or the input moves too fast. The response is pinned by the static input. This is referred to as the *pinned phase* (see Figs. 9(b) and 9(k)). As the moving velocity increases, stronger moving stimulus is needed to overcome the static interactions from the other module. When the moving input strength is sufficiently strong, module m is able to catch up with the moving input. This is the *tracking phase* with $\sigma_m^2 < \sigma_s^2$ (see Figs. 9(c) and 9(l)). In Figs. 9(a) and (j), in which module s excites module m , the phase boundaries are similar, with the pinned phase at low strength of the moving input (see Figs. 9(b) and 9(k)) and the tracking phase at high strength (see Figs. 9(c) and 9(l)).

On the other hand, when the module s inhibits module m , the phase boundaries in Fig. 9(d) are different from the other two cases and an *unpinned phase* exists at intermediate strength of the moving input. In Fig. 9(d), module m cannot build up stable and strong responses when the moving stimulus is very weak. This is

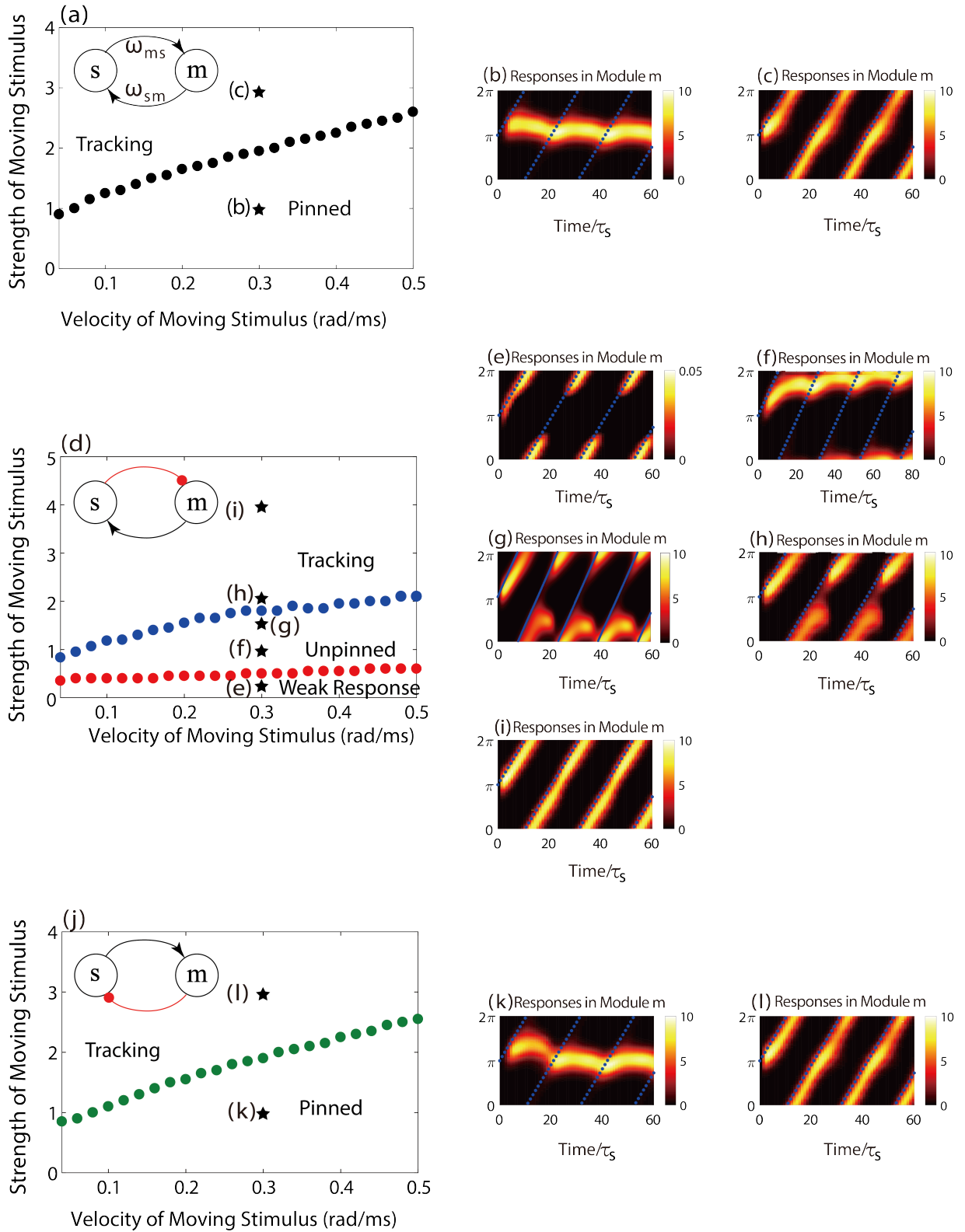


FIG. 9. The phase diagrams of the dynamical behaviors in module *m* with moving stimulus ((a), (d) and (j)) and network behaviors at selected locations. The static input I_{1ext} is fixed at the amplitude of 0.7, applied at position π , and the amplitudes of all couplings are fixed at 0.1. (b), (c) The firing rates (responses) of the bimodular CANN in (a) when I_{2ext} moves at speed of 0.3 rad/ms, and I_{2ext} is at the amplitude of 1 and 3 respectively. (e), (f), (g), (h) and (i) The firing rates (responses) of the bimodular CANN in (d) when I_{2ext} moves at speed of 0.3 rad/ms, and I_{2ext} is at the amplitude of 0.2, 1, 2 and 4 respectively. (k) and (l) The firing rates (responses) of the bimodular CANN in (j) when I_{2ext} moves at speed of 0.3 rad/ms, and I_{2ext} is at the amplitude of 1 and 3 respectively.

referred to as the *weak response phase*. Furthermore, due to the inhibitory inter-modular couplings ω_{ms} and the weak moving input, the responses are suppressed temporarily when the moving bump passes by the inhibitory static input (see Fig. 9(e)). This region of temporary suppression even extends slightly beyond the boundary of the weak response phase.

As the strength of moving stimulus increases, module m is able to build strong and stable responses. Due to the repulsion by the static input, the bump is repelled from the static input and drift with a low velocity, resulting in the *unpinned phase*. The drift velocity has the same direction as that of the moving input, with the bump attracted forward towards the moving input when the latter is ahead, or attracted backward towards the moving input when the latter is behind (see Fig. 9(f)). The bump motion is heavily affected by the presence of the static input, which forms a barrier to the bump motion, causing the drift of the bump to slow down and reverse from forward attraction to backward attraction.

As the moving input strength continues to increase, the bump trajectory follows the moving input closer. As a result, the forwardly-attracted segment of the bump trajectory and the backwardly-attracted segment become disconnected, A discontinuous jump of the center of mass of the bump can be observed (see Fig. 9(g)). On further increase of the moving input strength, the moving bump is able to overcome the barrier of the static input, and the two segments of the bump trajectory reconnect. However, the reconnection takes place in the forward direction, in contrast to the backward connection when the moving input strength is weak (see Fig. 9(h)). Hence, the bump is able to catch up with the moving input, and the network enters the tracking phase (see Fig. 9(i)) with $\sigma_m^2 < \sigma_s^2$.

Figure 9 summarizes the tracking dynamics of the bimodular CANNs under weak inter-modular couplings. As we have shown, a pair of inhibitory and excitatory weak inter-modular couplings can give rise to a rich spectrum of behaviors due to the competition between the direct external input and the indirect input through the inter-modular couplings.

V. SENSORY ILLUSION

Understanding the rich dynamics of bimodular networks can assist us in studying the multisensory information processing in the neural circuits. The brain receives different kinds of signals via distinct senses from surrounding environment, and generates appropriate responses after integration of the received information. There have been extensive studies focusing on the multisensory integration of different modes of signals, such as visual-vestibular [36, 37], visual-auditory [38, 44], and so forth [19, 24, 35, 39, 45, 46]. In this paper, we take ‘Motion-Bounce Illusion’ [30, 32, 47] experiment as an example, which incorporates visual and auditory signals, to elucidate how bimodular CANNs explain the experi-

ment.

The sketch of the ‘Motion-Bounce Illusion’ experiment is shown in Fig. 10. The subject first sees two balls located at point A and B respectively. When the experiment starts, the two balls begin to move towards the diagonal points C and D respectively with the same velocities. In test 1, when the two balls meet each other at the center point O, they keep the original velocities and moving directions, moving to the destination points. In test 2, when the two balls meet each other at the center point O, there will be a brief auditory input presented concurrently, sounding like ‘tink’, meanwhile the two balls still keep the original speeds and moving directions, moving towards points C and D respectively.

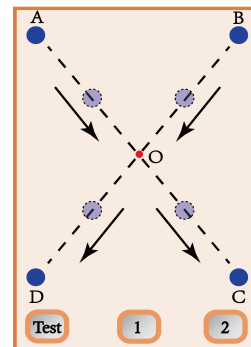


FIG. 10. The sketch map of the ‘Motion-Bounce Illusion’ experiment.

According to experimental results, the majority of observers reported in test 1 that they perceived the two balls streaming through each other, rather than colliding or bouncing off when they met at the center point O. In test 2, although the motions of the balls are the same, there is a considerable fraction of observers reporting that they perceived the two balls bounced off each other instead of streaming through. That is, the trajectories of the two balls become ‘><’, different from the ‘X’ shape in test 1.

We use a bimodular CANN to model the visual and auditory modules. In the visual module, we have a moving input with two peaks approaching each other with the same velocity. In the auditory module, we have a momentary static input simulating the brief auditory ‘tink’.

To quantify the perception of ‘streaming through’ and ‘bouncing off’, we introduce two reference patterns to represent them. The single-bump profile in Fig. 11(a) corresponds to the situation in which two balls overlap with each other completely at the meeting point O. The two-bump profile in Fig. 11(b) represents the situation that the two balls bounce off so that the observers can see two balls at the meeting point O. Based on these two reference patterns, we are able to calculate the bouncing ratio (BR) defined by

$$BR = \frac{P_B}{P_S + P_B}, \quad (13)$$

where P_S and P_B are the projections of the network responses at the meeting point to the respective reference patterns (S: streaming through, B: bouncing off) computed by

$$\begin{aligned} P_B &= \sum_{i=1}^N R_i \frac{M_{B_i}}{|M_B|}, \\ P_S &= \sum_{i=1}^N R_i \frac{M_{S_i}}{|M_S|}, \end{aligned} \quad (14)$$

in which R_i indicates the response of neuron i in the visual module at the meeting point O, N is the number of neurons in each module. M_{B_i} and M_{S_i} denotes the reference patterns at neuron i .

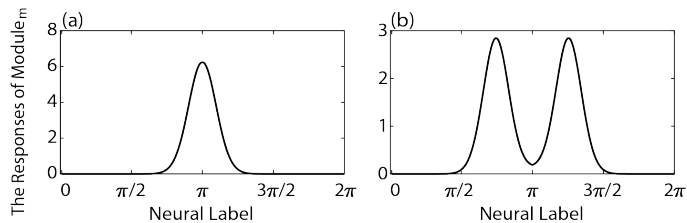


FIG. 11. The reference patterns in simulations of Motion-Bounce Illusion. (a) Reference pattern of streaming through. (b) Reference pattern of bouncing off. The central minimum is 3% of the two maxima.

In simulations, according to experiments [47], for visual module, we set the moving velocities of two visual cues are both 0.02 rad/ms. The duration of the auditory signal is 6 ms, which is present 6 ms before two balls collide. Both of auditory inputs and visual inputs are at same amplitudes of 1.2. We tried different couplings from visual module to auditory module, and found that only under the excitatory ω_{AV} couplings can the network model simulate the experiments very well, therefore we set the $\omega_{AV} = 0.1$. This also indicates that in this sensory illusion experiment, the functional inter-modular couplings from visual module to auditory module in brain are likely also excitatory. The rest of the network parameters are the same as in Fig. 9(d). We obtain the simulation results shown in Fig. 12. Each point denotes a BR value when the two balls meet at center point O. As the ‘tink’ sound increases the perception of bouncing off, ω_{VA} is set to be negative. While the visual cues have no inhibition effects on audition, the couplings from visual to auditory modality ω_{AV} are set to be excitatory. When ω_{VA} increases, the BR values also increase, indicating that the observers are more likely to sense the ‘bouncing illusion’. Furthermore, since the BR values remains effectively independent of the auditory input, it can be concluded that BRs are independent of the magnitudes of the auditory inputs.

We compare our simulation results with the ‘Motion-Bounce Illusion’ experimental results [30–32, 47]. In the experiment, the bouncing ratio increases by around 80% when the ‘tink’ sound is present, improving notably when compared with the case in the absence of the auditory

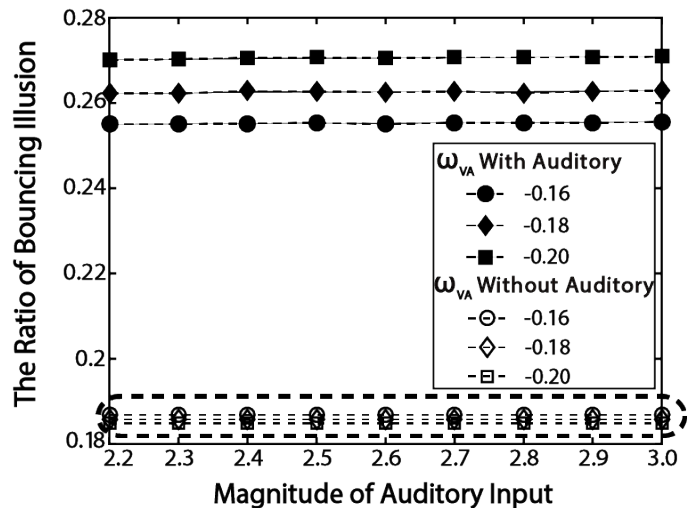


FIG. 12. The BRs under different inter-modular couplings and auditory input strengths. The region enclosed by the dashed lines denotes the simulation results without auditory inputs.

input. In the simulation, the increase of the bounding ratios are around 50%, which is comparable to the experiment results. Therefore the bimodular CANNs can be a useful modeling tool for comparison with experiments.

VI. CONCLUSIONS

We have generalized the study of unimodular CANNs to bimodular CANNs, endowing the network with the capacity to incorporate two sensory modalities. The inter-modular couplings in bimodular CANNs play important roles in determining the dynamics of the network (Fig. 3 and Fig. 4). Excitatory inter-modular couplings result in enhancing and attracting the responses of the other module, while inhibitory inter-modular couplings lead to suppressing and repelling effects for both static and moving inputs. The network behavior is determined by the interplay of the input strengths, their disparity, speed (for moving inputs) and the inter-modular couplings. The most interesting case is the bimodular CANN with a pair of excitatory and inhibitory inter-modular couplings. For static inputs at high disparity, it exhibits anomalous behavior with the inhibited module having stronger-than-expected output than the excited module. For static and moving inputs to the excited and inhibited modules respectively, a series of drifting responses with continuous and discontinuous evolution occur when the moving input strength increases and finally arriving at the tracking phase.

We have shown that bimodular networks are relevant to issues in neuroscience and neural information processing. In the study of static inputs, they are useful in modeling causal inference. Bimodular networks connected by excitatory inter-modular couplings yield integrated outputs at low disparity and segregated outputs

at high disparity, This provides a neural substrate for causal inference based on a wide range of prior distributions. Bimodular networks with a pair of excitatory and inhibitory inter-modular couplings can also be used to model causal inference in which one channel is subordinate to the other. In this paper we have not discussed bimodular networks with inhibitory couplings, but they are already important components in models of competitive decision making [48–50]. Using bimodular networks with dynamical inputs, we have also modeled multisensory psychophysics experiments such as the motion-bounce illusion experiment and predict that the psychophysical effect is robust in a wide range of the magnitude of the auditory input.

Multisensory interactions has been an important issue which has been studied extensively. Figuring out how brain processes multisensory signals is an important topic not only in modeling the functions of the brain, but also in the technological applications of neural computation. It has been commonly recognized that excitatory couplings between modules are important when the brain deals with different channels of signals that are correlated [51], and the inhibitory couplings are important when the brain processes signals that are uncorrelated or anti-correlated [23, 52]. There have been experiments

finding ‘congruent’ and ‘opposite’ cells [36], with which the neural system responds to signals with different disparities can be rather diverse in experiments integrating visual and vestibular signals in the monkey’s brain. In a recently proposed model explaining the functions of the congruent and opposite cells in Bayes-optimal inference, the inter-modular couplings play an important role. Recent work also showed that the network structure to achieve Bayes-optimal performance incorporating both excitatory or inhibitory couplings depends on the prior distribution of the signals [53]. While most of the studies focus on the steady state behaviors of the neural system, our work shows that dynamical and temporal behaviors are also important, and the transient behaviors of the neural system may also be useful in conveying information between the sensory modalities. Experiments based on temporal integration, such as the moving-bounce illusion experiment, can also be designed to further study the multisensory information processing.

Acknowledgments

This work is supported by grants from the Research Grants Council of Hong Kong (grant numbers 16322616, 16306817 and 16302419).

-
- [1] D.J. Amit, *Modeling brain function: The world of attractor neural networks* (Cambridge University Press, Cambridge, UK, 1992).
- [2] W. Gerstner, W. M. Kistler, R. Naud, and L. Paninski, *Neuronal dynamics: From single neurons to networks and models of cognition* (Cambridge University Press, Cambridge, UK, 2014).
- [3] P. Dayan and L. F. Abbott, *Theoretical Neuroscience*, Vol. 806 (2001).
- [4] R. Ben-Yishai, D. Hansel, and H. Sompolinsky, Traveling waves and the processing of weakly tuned inputs in a cortical network module. *J. Comput. Neurosci.* 4(1), 57-77 (1997).
- [5] H. R. Wilson and J. D. Cowan, Excitatory and inhibitory interactions in localized populations of model neurons, *Biophys. J.* 12(1), 1-24 (1972).
- [6] S. I. Amari, Dynamics of pattern formation in lateral-inhibition type neural fields, *Biol. Cybern.* 27(2), 77-87 (1977).
- [7] J. H. Maunsell and D. C. Van Essen, Functional properties of neurons in middle temporal visual area of the macaque monkey. I. Selectivity for stimulus direction, speed, and orientation, *J. Neurophysiol.* 49(5), 1127-1147 (1983).
- [8] S. Deneve, P. E. Latham and A. Pouget, Reading population codes: a neural implementation of ideal observers, *Nat. Neurosci.* 2(8), 740-745 (1999).
- [9] A. Samsonovich and B. L. McNaughton, Path integration and cognitive mapping in a continuous attractor neural network model, *J. Neurosci.* 17(15), 5900-5920 (1997).
- [10] M. Camperi and X. J. Wang, A model of visuospatial working memory in prefrontal cortex: recurrent network and cellular bistability, *J. Comput. Neurosci.* 5(4), 383-405 (1998).
- [11] S. Wu, S. I. Amari and H. Nakahara, Population coding and decoding in a neural field: a computational study, *Neural Comput.* 14(5), 999-1026 (2002).
- [12] S. Wu and S. I. Amari, Computing with continuous attractors: Stability and online aspects, *Neural Comput.* 17(10), 2215-2239 (2005).
- [13] S. Wu, K. Hamaguchi and S. I. Amari, Dynamics and computation of continuous attractors, *Neural Comput.* 20(4), 994-1025 (2008).
- [14] C. C. A. Fung, K. Y. M. Wong and S. Wu, Dynamics of neural networks with continuous attractors, *EPL* 84(1), 18002 (2008).
- [15] C. C. A. Fung, K. Y. M. Wong and S. Wu, A moving bump in a continuous manifold: A comprehensive study of the tracking dynamics of continuous attractor neural networks, *Neural Comput.* 22(3), 752-792 (2010).
- [16] C. C. A. Fung, K. Y. M. Wong, H. Wang and S. Wu, Dynamical synapses enhance neural information processing: gracefulness, accuracy, and mobility, *Neural Comput.* 24(5), 1147-1185 (2012).
- [17] C. C. A. Fung, H. Wang, K. Lam, K. Y. M. Wong, and S. Wu, Resolution enhancement in neural networks with dynamical synapses, *Front. Comput. Neurosci.* 7 (2013).
- [18] C. S. Zhou, L. Zemanov, G. Zamora, C. C. Hilgetag and J. Kurths, Hierarchical organization unveiled by functional connectivity in complex brain networks, *Phys. Rev. Lett.* 97(23), 238103 (2006).
- [19] J. Driver and T. Noesselt, Multisensory interplay reveals crossmodal influences on ‘sensory-specific’ brain regions, neural responses, and judgments, *Neuron* 57(1), 11-23

- (2008).
- [20] C. R. Fetsch, G. C. DeAngelis and D. E. Angelaki, Bridging the gap between theories of sensory cue integration and the physiology of multisensory neurons, *Nat. Rev. Neurosci.* 14(6), 429-442 (2013).
- [21] T. R. Stanford, S. Quessy and B. E. Stein, Evaluating the operations underlying multisensory integration in the cat superior colliculus, *J. Neurosci.* 25(28), 6499-6508 (2005).
- [22] P. M. Jaekl and L. R. Harris, Auditoryvisual temporal integration measured by shifts in perceived temporal location, *Neurosci. Lett.* 417(3), 219-224 (2007).
- [23] W. H. Zhang, A. Chen, M. J. Rasch and S. Wu, Decentralized multisensory information integration in neural systems, *J. Neurosci.* 36(2), 532-547 (2016).
- [24] M. O. Ernst and M. S. Banks, Humans integrate visual and haptic information in a statistically optimal fashion, *Nature* 415(6870), 429-433 (2002).
- [25] C. C. A. Fung, K. Y. M. Wong and S. Wu, Tracking dynamics of two-dimensional continuous attractor neural networks, *J. Phys. Conf. Ser. Vol. 197, No. 1*, p. 012017 (2009).
- [26] C. C. A. Fung, K. Y. M. Wong, H. Z. Mao and S. Wu, Fluctuation-response relation unifies dynamical behaviors in neural fields, *Phys. Rev. E*, 92(2), 022801 (2015).
- [27] H. Wang, K. Lam, C. C. A. Fung, K. Y. M. Wong and S. Wu, Rich spectrum of neural field dynamics in the presence of short-term synaptic depression, *Phys. Rev. E*, 92(3), 032908 (2015).
- [28] L. Shams, Y. Kamitani and S. Shimojo, Illusions: What you see is what you hear, *Nature*, 408(6814), 788-788 (2000).
- [29] L. Shams, Y. Kamitani and S. Shimojo, Visual illusion induced by sound, *Brain Res. Cogn. Brain Res.* 14(1), 147-152 (2002).
- [30] S. Shimojo and L. Shams, Sensory modalities are not separate modalities: plasticity and interactions, *Curr. Opin. Neurol.* 11(4), 505-509 (2001).
- [31] S. Watkins, L. Shams, S. Tanaka, J. D. Haynes and G. Rees, Sound alters activity in human V1 in association with illusory visual perception, *Neuroimage*, 31(3), 1247-1256 (2006).
- [32] R. Sekuler, A. B. Sekuler and R. Lau, Sound alters visual motion perception, *Nature*, 385(6614), 308 (1997).
- [33] M. Carandini and D. J. Heeger, Normalization as a canonical neural computation, *Nat. Rev. Neurosci.* 13(1), 51-62 (2012).
- [34] W. H. Zhang and S. Wu, Neural information processing with feedback modulations, *Neural Comput.* 24(7), 1695-1721 (2012).
- [35] L. Shams and A. R. Seitz, Benefits of multisensory learning, *Trends Cogn. Sci.* 12(11), 411-417 (2008).
- [36] Y. Gu, D. E. Angelaki and G. C. DeAngelis, Neural correlates of multisensory cue integration in macaque MSTd, *Nat. Neurosci.* 11(10), 1201-1210 (2008).
- [37] K. Dokka, G. C. DeAngelis and D. E. Angelaki, Multisensory Integration of Visual and Vestibular Signals Improves Heading Discrimination in the Presence of a Moving Object, *J. Neurosci.* 35(40), 13599-13607 (2015).
- [38] S. Molholm, W. Ritter, D. C. Javitt and J. J. Foxe, Multisensory audiovisual object recognition in humans: a high-density electrical mapping study, *Cereb. Cortex* 14(4), 452-465 (2004).
- [39] C. R. Fetsch, A. Pouget, G. C. DeAngelis, G. C. and D. E. Angelaki, Neural correlates of reliability-based cue weighting during multisensory integration, *Nat. Neurosci.* 15(1), 146-154 (2012).
- [40] T. Ohshiro, D. E. Angelaki, D. E. and G. C. DeAngelis, A normalization model of multisensory integration, *Nat. Neurosci.* 14(6), 775 (2011).
- [41] A. Pouget, K. Zhang, S. Deneve and P. E. Latham, Statistically efficient estimation using population coding, *Neural Comput.* 10(2), 373-401 (1998).
- [42] S. Wu, H. Nakahara and S. I. Amari, Population coding with correlation and an unfaithful model, *Neural Comput.* 13(4), 775-797 (2001).
- [43] L. Shams and U. R. Beierholm, Causal inference in perception, *Trends Cogn. Sci.* 14(9), 425-432 (2010).
- [44] A. R. Seitz, R. Kim and L. Shams, Sound facilitates visual learning, *Curr. Biol.* 16(14), 1422-1427 (2006).
- [45] W. D. Hairston, M. T. Wallace, J. W. Vaughan, B. E. Stein, J. L. Norris and J. A. Schirillo, Visual localization ability influences cross-modal bias, *J. Cogn. Neurosci.* 15(1), 20-29 (2003).
- [46] B. Odegaard, D. R. Wozny and L. Shams, The effects of selective and divided attention on sensory precision and integration, *Neurosci. Lett.* 614, 24-28 (2016).
- [47] K. Watanabe, Crossmodal interaction in humans (Doctoral dissertation, California Institute of Technology) (2001).
- [48] X. J. Wang, Probabilistic decision making by slow reverberation in cortical circuits, *Neuron* 36(5), 955-968 (2002).
- [49] X. J. Wang, Decision making in recurrent neuronal circuits, *Neuron* 60(2), 215-234 (2008).
- [50] C. T. Wang, C. T. Lee, X. J. Wang, and C. C. Lo, Top-down modulation on perceptual decision with balanced inhibition through feedforward and feedback inhibitory neurons, *PLOS ONE* 8(4), e62379 (2013).
- [51] R. S. Kim, A. R. Seitz and L. Shams, Benefits of stimulus congruency for multisensory facilitation of visual learning, *PLOS ONE* 3(1), e1532 (2008).
- [52] W. H. Zhang, H. Wang, K. Y. M. Wong and S. Wu, 'Congruent' and 'Opposite' Neurons: Sisters for Multisensory Integration and Segregation, *NeurIPS* (pp. 3180-3188) (2016).
- [53] H. Wang, W. H. Zhang, K. Y. M. Wong and S. Wu, How the prior information shapes neural networks for optimal multisensory integration, (14th International Symposium on Neural Networks (ISNN)), Sapporo, Japan (2017).

APPENDIX: CAUSAL INFERENCE IN AN OPPOSITELY COUPLED BIMODULAR NETWORK

Following [23], we consider a generic prior of two real-valued stimuli s_1 and s_2 described by

$$p(s_1, s_2) = N(0, \sigma_s^2), \quad (\text{A1})$$

where $N(0, \sigma_s^2)$ is a normal distribution with mean 0 and variance σ_s^2 . Instead of the independent likelihood considered in [23], we focus on the case that the cues z_1 and z_2 are generated by the stimuli given by the correlated likelihood

$$p(z_1, z_2 | s_1, s_2) \propto \exp \left[-\frac{1}{2} (\mathbf{Z} - \mathbf{S})^T (\mathbf{C}^{-1}) (\mathbf{Z} - \mathbf{S}) \right] \quad (\text{A2})$$

where $c_{ij} = \langle (z_i - s_i)(z_j - s_j) \rangle$. Using Bayes' rule, the posterior probability is given by

$$p(s_1, s_2 | z_1, z_2) \propto p(z_1, z_2 | s_1, s_2) p(s_1, s_2). \quad (\text{A3})$$

In a bimodular network, the posterior estimate of s_1 is given by

$$p(s_1 | z_1, z_2) = \int ds_2 p(s_1, s_2 | z_1, z_2). \quad (\text{A4})$$

Noting that the integrand is a Gaussian function, we obtain the mean and variance of the posterior distribution given by

$$\hat{s}_1 = \frac{(c_{22} - c_{11} + \sigma_s^2)z_1 + (c_{11} - c_{12})z_2}{c_{11} + c_{22} - 2c_{12} + \sigma_s^2}, \quad (\text{A5})$$

$$\hat{\sigma}_1^2 = \frac{c_{11}c_{22} - c_{12}^2 + c_{11}\sigma_s^2}{c_{11} + c_{22} - 2c_{12} + \sigma_s^2}. \quad (\text{A6})$$

The posterior mean of s_2 can be obtained similarly. To relate the inference of a module to its direct input and the inference of the other module, we have

$$\hat{s}_1 = \frac{\sigma_s^2}{\sigma_s^2 + c_{11} - c_{12}} z_1 + \frac{c_{11} - c_{12}}{\sigma_s^2 + c_{11} - c_{12}} \hat{s}_2, \quad (\text{A7})$$

$$\hat{s}_2 = \frac{\sigma_s^2}{\sigma_s^2 + c_{22} - c_{12}} z_2 + \frac{c_{22} - c_{12}}{\sigma_s^2 + c_{22} - c_{12}} \hat{s}_1. \quad (\text{A8})$$

Note that there is an important difference with the case of independent likelihoods in which $c_{12} = 0$. Instead of having \hat{s}_2 positively weighted in \hat{s}_1 and vice versa, there exist likelihood functions in which $c_{11} - c_{12}$ and $c_{22} - c_{12}$ have opposite signs. For example, for the following correlated noise, input 1 is subordinate to input 2,

$$s_1 - z_1 = t_1, \quad s_2 - z_2 = \frac{t_1}{2}, \quad t_1 \sim N(0, 1). \quad (\text{A9})$$

This results in

$$c_{11} - c_{12} = \frac{1}{2}, \quad c_{22} - c_{12} = -\frac{1}{4}. \quad (\text{A10})$$

Next, we will show that this setting can be implemented by a bimodular network in which the couplings from module 2 to 1 are excitatory, and the couplings from module 1 to 2 are inhibitory. Consider network solutions of the form, for $i = 1, 2$,

$$U_i(x_i) = U_{0i} \exp \left[-\frac{(x_i - \hat{s}_i)^2}{4a^2} \right]. \quad (\text{A11})$$

Substituting the solution into the Eq. (8) and integrating over x_1 and x_2 in the first and second equations respectively, we obtain

$$U_{01} = \frac{\omega_{11}}{\sqrt{2}} \frac{U_{01}^2}{B_1} + \frac{\omega_{12}}{\sqrt{2}} \frac{U_{02}^2}{B_2} + I_{01}, \quad (\text{A12})$$

$$U_{02} = \frac{\omega_{21} U_{01}^2}{\sqrt{2} B_1} + \frac{\omega_{22} U_{02}^2}{\sqrt{2} B_2} + I_{02}, \quad (\text{A13})$$

where $B_i = 1 + kU_{0i}^2/8$ for $i = 1, 2$. Substituting Eq. (A11) into Eq. (8), multiplying both sides by x_1 and x_2 in the first and second equations respectively, integrating over x_1 and x_2 in the respective equations, and using Eqs. (A12) and (A13), we obtain

$$\hat{s}_1 = \frac{\omega_{12} U_{02}^2}{\omega_{12} U_{02}^2 + \sqrt{2} B_2 I_{01}} \hat{s}_2 + \frac{\sqrt{2} B_2 I_{01}}{\omega_{12} U_{02}^2 + \sqrt{2} B_2 I_{01}} z_1, \quad (\text{A14})$$

$$\hat{s}_2 = \frac{\omega_{21} U_{01}^2}{\omega_{21} U_{01}^2 + \sqrt{2} B_1 I_{02}} \hat{s}_1 + \frac{\sqrt{2} B_1 I_{02}}{\omega_{21} U_{01}^2 + \sqrt{2} B_1 I_{02}} z_2. \quad (\text{A15})$$

Comparing these equations with Eqs. (A7) and (A8), we see that when the causal inference of an input is subordinate to another such as in the example of Eq. (A9), the network implementation can be achieved by having an excitatory ω_{12} and an inhibitory ω_{21} .